mater.scichina.com link.springer.com

Published online 27 May 2020 | https://doi.org/10.1007/s40843-020-1339-8
Sci China Mater 2020, 63(9): 1808–1817

Facile thermal decomposition synthesis of sub-5 nm nanodots with long-lived luminescence for autofluorescence-free bioimaging

Xiaobo Lv[1†], Na Chen[1†], Jie Wang[1] and Quan Yuan[1,2*]

ABSTRACT **Persistent nanophosphors can remain luminescent after the removal of the excitation. Persistent nanophosphors exhibit great advantages in biomedical fields, particularly in autofluorescence-free bioimaging and in-site-excitation-free photo-theranostics. Despite the great promise of persistent nanophosphors in biomedicine, studies on the controlled synthesis of persistent nanophosphors are limited. Herein, a metal acetylacetonate-based thermal decomposition method was developed for the synthesis of ultra-small persistent luminescence nanodots (PLNDs). The PLNDs display uniform size, good dispersibility and strong persistent luminescence. The luminescent properties of the PLNDs can be readily regulated by ion doping. The thermal decomposition method shows excellent versatility in the synthesis of PLNDs including gallate, sulfide and fluoride. Due to their ultra-small size and surface adsorbed hydrophobic ligand, the PLNDs can be easily integrated with liposomes to construct a stable and biocompatible persistent luminescent nanoplatform for biomedical applications. This work puts forwards a versatile method for the controlled synthesis of ultra-small persistent nanophosphors, and it may further contributes to the areas ranging from biosensing to cancer therapy.**

Keywords: persistent luminescence, thermal decomposition, nanoparticles, bioimaging

INTRODUCTION

Persistent luminescence describes the phenomenon that luminescence remains after the excitation is ceased [1–4]. Persistent nanophosphors have recently attracted intensive attention in applications ranging from biosensing [5–8] to cancer therapy [9–13]. In biosensing and bioimaging, considering that the fluorescence lifetime of background fluorophores in biological samples is usually in the nanosecond range, persistent nanophosphors with ultra-long luminescence lifetime can effectively avoid the background fluorescence interference by time-gating [5,6], thus significantly improving the sensitivity of biosensing and bioimaging. Besides, persistent nanophosphors are also widely studied in in-site excitation-free photo-theranostics because persistent nanophosphors can store the excitation energy and gradually release the energy for photo-therapy after the stoppage of light irradiation [10,11]. Persistent nanophosphors can efficiently avoid the photo-induced damage of tissues, exhibiting good potentials in photodynamic therapy and photothermal therapy. Despite the great promise of persistent nanophosphors in biomedical applications, there are limited reports regarding the controlled synthesis of persistent nanophosphors [14–17]. Currently, most persistent nanophosphors are synthesized through "top-down" methods such as wet grinding [16], resulting in nanoparticles with non-uniform size distribution, poor surface modification and dispersion. Only a few studies reported the direct synthesis of persistent nanophosphors with solvothermal method. Typically, Li *et al.* [18] demonstrated the aqueous-phase synthesis of sub-10 nm $ZnGa_2O_4$:Cr persistent nanophosphors. Zhou *et al.* [19] pioneered a solvothermal liquid-solid-solution method for the synthesis of $ZnGa_2O_4$:Cr nanoparticles with bright

[1] Key Laboratory of Analytical Chemistry for Biology and Medicine (Ministry of Education), College of Chemistry and Molecular Sciences, Wuhan University, Wuhan 430072, China
[2] Institute of Chemical Biology and Nanomedicine, State Key Laboratory of Chemo/Biosensing and Chemometrics, College of Chemistry and Chemical Engineering, Hunan University, Changsha 410082, China
[†] These authors contributed equally to this work.
[*] Corresponding author (email: yuanquan@whu.edu.cn)

persistent luminescence. The limited research on the controlled synthesis of persistent nanophosphors has severely impeded the application of persistent nanophosphors. Therefore, it is of great importance to develop facile and efficient methods for the synthesis of persistent nanophosphors.

Thermal decomposition is a widely used synthesis method that involves the thermolysis of precursors in the high-boiling-point solvents and the subsequent formation of nanocrystals [20–22]. As the reaction temperature increases, the organic precursors are dissolved into the solution in the presence of surfactants and then decomposed to form crystal nuclei [20]. During the growth of the crystals, the surfactant could bind to specific crystal plane and direct the further growth of the crystals [22]. Thermal decomposition synthesis exhibits advantages of easy operation, time saving, precise control in the size, shape and morphology. Benefiting from these merits, thermal decomposition has been widely used in the synthesis of nanomaterials including upconversion nanoparticles [23–25], magnetic nanoparticles [26] and rare-earth oxide nanocrystals [27].

In this work, we reported a metal acetylacetonate-based thermal decomposition method for the controlled synthesis of ultra-small persistent luminescence nanodots (PLNDs). The prepared PLNDs show uniform size distribution and good dispersibility. Strong persistent luminescence and long decay time are observed in the PLNDs. Besides, the persistent luminescence properties of the PLNDs can be well modulated *via* ion doping. Moreover, the metal acetylacetonate-based thermal decomposition method shows good versatility in the synthesis of different types of PLNDs, including gallate, sulfide and fluoride. Due to their ultra-small size, the hydrophobic ligand-stabilized PLNDs can be easily incorporated into the gap of lipid bilayer for biomedical applications. Results show that PLNDs-incorporated liposomes display high sensitivity in autofluorescence-free deep-tissue imaging. This work provides an efficient strategy for the controlled synthesis of persistent nanophosphors, and it may further promote the applications of persistent nanophosphors in fields including biosensing, bioimaging, disease therapy, and photocatalysis.

EXPERIMENTAL SECTION

Materials

Zinc acetylacetonate hydrate ($Zn(acac)_2$), gallium (III) 2,4-pentandionate ($Ga(acac)_3$), chromium (III) acetylacetonate ($Cr(acac)_3$), aluminum acetylacetonate ($Al(acac)_3$), scandium (III) 2,4-pentandionate hydrate ($Sc(acac)_3$) and calcium acetylacetonate ($Ca(acac)_2$) were purchased from Alfa Aesar Chemistry Co., Ltd. (China). Oleylamine (OM, 90%), oleic acid (OA, 90%), 1-octadecene (ODE, ≥90%), sulfur powders (S, AR), ammonium fluoride (AR, 98%) and sodium hydroxide (NaOH, AR, 96%) were purchased from Aldrich (China). Absolute ethanol (C_2H_6O, ≥99.7%), cyclohexane (C_6H_{12}, ≥99.5%), methanol (CH_4O, ≥99.5%), acetone (C_3H_6O, ≥99.5%) and cholesterol were purchased from Sinopharm Chemical Reagent Co. Ltd. (China). The 1,2-dipalmitoyl-*sn*-glycero-3-phosphocholine (DPPC) and 1,2-dipalmitoyl-*sn*-glycero-3-phosphoethanolamine-*N*-[methoxy-(polyethyleneglycol)-amine] (DPPE-PEG-NH_2, *M*w 2000) were provided by Avanti Polar Lipids, Inc. (China). All reagents were used as received without further purification.

Preparation of $ZnGa_2O_4$:Cr, $ZnGa_2O_4$:Al_x,Cr (x=0.025, 0.05, 0.075, 0.1) and $ZnGa_2O_4$:Sc_x,Cr (x=0.025, 0.05, 0.075, 0.1) PLNDs

In a typical synthesis protocol, $Zn(acac)_2$ (0.4 mmol), $Ga(acac)_3$ (0.8 mmol), $Cr(acac)_3$ (0.002 mmol), OM (10 mL) were mixed in a 50-mL three-necked flask at room temperature under stirring. Then the solution was heated to 120°C and maintained at this temperature for 30 min in vacuum with vigorous stirring for the removal of water and other low-boiling-point impurities. After that, the solution was heated to 315°C at the rate of 20°C min^{-1} under a high-purity argon atmosphere. The transparent yellow solution became turbid when the reaction temperature reached up to about 250°C. After reacting at 315°C for 45 min, $ZnGa_2O_4$:Cr (ZGO:Cr) PLNDs were obtained. The ZGO:Cr PLNDs were precipitated with ethanol and further collected by centrifugation and washed three times with ethanol and cyclohexane (3:1) at 10,000 r min^{-1} for 10 min. Finally, the purified ZGO:Cr PLNDs were re-dispersed in cyclohexane. The further doping of Al or Sc in ZGO:Cr PLNDs was realized with the same procedures except for the addition of $Al(acac)_3$ or $Sc(acac)_3$ precursors.

Preparation of ZnS:Cr PLNDs

The synthetic method of ZnS:Cr PLNDs were similar to that of the ZGO:Cr PLNDs. Firstly, $Zn(acac)_2$ (1 mmol), sulfur powders (1 mmol), $Cr(acac)_3$ (0.005 mmol), OM (6 mL) and ODE (6 mL) were mixed in a 50-mL three-necked flask at room temperature with stirring. Then the mixed system was heated to 120°C and kept at this temperature for 30 min in vacuum with vigorous stirring.

After that, the solution was heated to 300°C at a rate of 20°C min^{-1} under a high-purity argon atmosphere. The ZnS:Cr PLNDs were obtained after reacting at 300°C for 60 min. The prepared ZnS:Cr PLNDs were precipitated with ethanol, followed by repeated centrifugations (10,000 r min^{-1}, 10 min) and washing with the mixture of ethanol and cyclohexane (3:1) for three times. Finally, the purified ZnS:Cr PLNDs were re-dispersed in cyclohexane.

Preparation of CaF_2 PLNDs

The synthetic method of CaF_2 NCs was similar to that of ZnS:Cr PLNDs. Firstly, $Ca(acac)_2$ (1 mmol), OA (5 mL) and ODE (15 mL) were mixed in a 50-mL three-necked flask at room temperature under stirring. Then the mixed system was heated to 160°C and kept at this temperature for 30 min in vacuum with constant stirring. The mixture gradually transformed into clear yellowish-brown solution. Then the mixture was cooled down to room temperature. After that, 10 mL of methanol solution including 2.5 mmol NH_4F and 2.5 mmol NaOH was injected into the mixture and the solution was heated to 60°C for 30 min with constant stirring to remove methanol. Thereafter, the resulting solution was heated to 280°C for 60 min under a high-purity argon atmosphere. The obtained CaF_2 PLNDs were precipitated with acetone. The CaF_2 PLNDs were further washed with the mixture of ethanol and cyclohexane for three times. Finally, the purified CaF_2 PLNDs were re-dispersed in cyclohexane.

Preparation of the liposome@ZGO:Al,Cr nanostructures

Firstly, the liposomes were synthesized by thin lipid film-hydrated methods according to the previous reports. Specifically, DPPC, cholesterol, and DPPE-PEG-NH_2 (100:50:5, molar ratio, 26 mg in total) were mixed in 3 mL of chloroform and then the mixture was added into a round-bottom flask followed by evaporation using a rotovaporator (30 min at 65°C). Then a lipid film formed on the flask wall. Thereafter, 1 mL of phosphate buffer saline (PBS, 0.01 mol L^{-1}, pH 7.4) was added to hydrate the formed film, followed by stirring for 10 min at 65°C. Next, the solution was stirred for 45 min at room temperature, and sonicated for 4 min. After that, 0.106 mL of ethanol was added to the phospholipids suspension, and the suspension was stirred at 150 r min^{-1} at 4°C for 24 h. Further, the suspension was centrifuged and washed three times with PBS (0.01 mol L^{-1}, pH 7.4) to remove ethanol. Finally, the blank liposome was obtained after being dispersed in PBS (0.01 mol L^{-1}, pH 7.4). The ZGO:$Al_{0.075}$, Cr PLNDs were dried in air at 60°C overnight for the preparation of the liposome@ZGO:Al,Cr nanostructures. Briefly, 1 mg of ZGO:$Al_{0.075}$,Cr was dispersed into 0.5 mL of PBS (0.01 mol L^{-1}, pH 7.4) and then the mixture was mixed with 1 mL of the obtained phospholipid suspension. Thereafter, the solution was heated at 50°C for 2 h under vortex mixing. Finally, the liposome@ZGO:Al,Cr nanostructures were obtained after centrifugation and redispersing in PBS (0.01 mol L^{-1}, pH 7.4).

Autofluorescence-free bioimaging

Firstly, the liposome@ZGO:Al,Cr suspension was irradiated with UV lamp (254 nm) for 3 min. And then, 50 μL of the suspension (containing about 15 μg ZGO:Al, Cr nanoparticles) was injected into a piece of pork at 1 cm deep. The images of the persistent luminescence signal from the pork were collected with an IVIS Lumina XR Imaging System under bioluminescence mode.

Sample testing

In the measurement of the persistent luminescence decay images with the IVIS Lumina XR Imaging System, 45 mg solid powder of each sample was used for the measurement of phosphorescence spectrum and persistent luminescence decay.

Characterizations

The morphology and size of the PLNDs were measured on a transmission electron microscope (JEOL, JEM-2100, Japan). The crystal structures of the PLNDs were analyzed by a Bruker X-ray diffractometer (Bruker, D8 Advance, Germany). The phosphorescence spectra of the PLNDs were obtained with a fluorescence spectrometer (Hitachi, F-4600, Japan). The persistent luminescence decay images of the PLNDs and the liposome@ZGO:Al, Cr nanostructures were obtained by an IVIS Lumina XR Imaging System (Caliper, USA). The energy dispersive X-ray spectroscopy (EDS) images of PLNDs were obtained by a FEI Verios 460 HR-FESEM (USA). The images of the liposome@ZGO:Al,Cr nanostructures were characterized with a confocal laser scanning microscope (FV1200, Olympus, Japan) with 405 nm laser excitation. The size of the liposome@ZGO:Al,Cr nanostructures were measured with an atomic force microscope (AFM, Veeco, Nano-Man) by Bruker Multimode 8 operated in tapping mode. Solid powders (45 mg) of ZGO:Cr, ZGO:Al,Cr, ZGO:Sc, Cr, ZnS:Cr and CaF_2 PLNDs were used in the measurement of their phosphorescence spectra and the persistent luminescence decay images. The dispersion of liposome@ZGO:Al,Cr in PBS was used in the measurement of its phosphorescence spectra and the persistent lumi-

nescence decay images.

RESULTS AND DISCUSSION

The thermal decomposition method developed in this study is illustrated in Scheme 1. Metal acetylacetonates were utilized as the precursors, and OM was used as the solvent. Previous studies reported that metal acetylacetonates showed mild decomposition speed during thermal reaction, and they have been widely used in the synthesis of nanoparticles with controllable size and shape [20]. The OM, which can act as both the reacting solvent and the stabilizer [21], was used to avoid the aggregation of the nanocrystals for the generation of uniformly sized PLNDs. The thermal decomposition reaction was preceded at 300°C under argon atmosphere. With the rapid increase of reaction temperature to 300°C, the metal acetylacetonate precursors were decomposed to form crystal nuclei. The crystal nuclei continued to grow into persistent luminescence nanocrystals that were stabilized by OM. The as-prepared PLNDs can trap the energy of incident light within the crystal defects, and further release the trapped energy by irradiation after the incident light is switched off. Gallate, sulfide and fluoride PLNDs were prepared with the thermal decomposition method. All of the PLNDs show uniform size, good dispersibility and pronounced persistent luminescence.

Transmission electron microscopy (TEM) was used to study the morphology of the as-prepared ZGO:Cr PLNDs. As shown in Fig. 1a and Fig. S1, the ZGO:Cr PLNDs exhibit excellent dispersibility and are highly uniform with a cubic shape. High resolution TEM (HRTEM) image in the inset of Fig. 1a shows that the ZGO:Cr PLNDs display well-defined crystalline fringe with a *d*-spacing of 0.29 nm, corresponding to the (113) plane of ZGO:Cr crystal. The size distribution in Fig. 1b further shows that the average size of the ZGO:Cr PLNDs is about 5 nm. Fig. 1c presents the X-ray diffraction (XRD) pattern of the ZGO:Cr PLNDs, which presents the characteristic diffraction of ZGO crystal. EDS measurement further confirms the presence of Cr in the ZGO:Cr PLNDs (Fig. 1d), suggesting the successful doping of other ions in PLNDs with the developed thermal de-

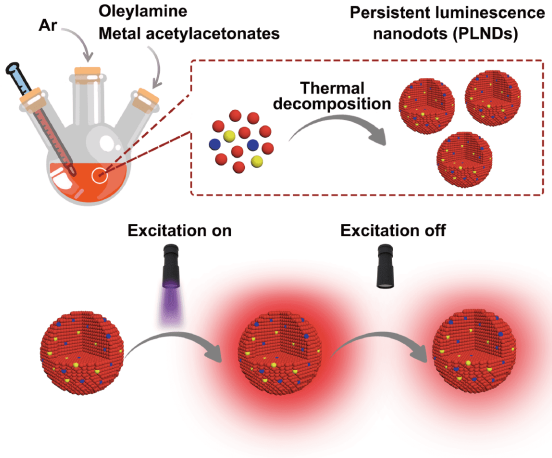

Scheme 1 Schematic illustration of the synthesis of PLNDs *via* a thermal decomposition method.

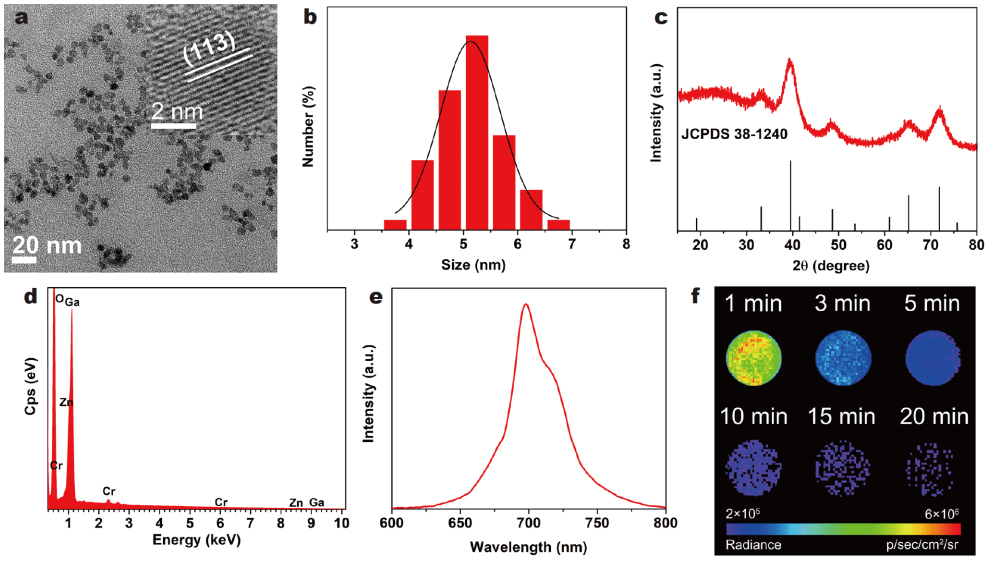

Figure 1 (a) TEM and HRTEM (inset) images of the ZGO:Cr PLNDs. (b) The size distribution of the ZGO:Cr PLNDs. (c) XRD pattern and (d) EDS analysis of the ZGO:Cr PLNDs. (e) Phosphorescence spectrum and (f) persistent luminescence decay images of the ZGO:Cr PLNDs.

composition method. The luminescence properties of the ZGO:Cr PLNDs were systematically investigated. As shown in Fig. 1e, a strong emission peak at about 700 nm is observed in the phosphorescence spectrum of ZGO:Cr PLNDs, which is corresponding to the typical $^2E \rightarrow {}^4A_2$ emission of Cr^{3+} ions. The persistent luminescence in the ZGO:Cr PLNDs was further measured with an IVIS Lumina XR imaging system. After the light source is ceased, ZGO:Cr PLNDs display obvious persistent luminescence. Even after 20 min of decay, the persistent luminescence of ZGO:Cr PLNDs can still be clearly observed (Fig. 1f). The corresponding fitted decay curve further shows the ultra-long decay of persistent luminescence in the ZGO:Cr PLNDs (Fig. S2). All these results indicate that ultra-small ZGO:Cr PLNDs were successfully prepared by the thermal decomposition method.

Ion doping is an efficient strategy to modulate the luminescence properties of phosphors [28–31]. The thermal decomposition method was further used to prepare doped ZGO:Cr PLNDs. Al^{3+} and Sc^{3+} that have equal charges with Ga^{3+} in the ZGO:Cr were chosen as the doping ions, respectively. Fig. 2a and Fig. S3 show that the Al^{3+}-doped ZGO:Cr (ZGO:$Al_{0.075}$,Cr) PLNDs exhibit excellent monodispersity and uniform morphology. The HRTEM image of ZGO:$Al_{0.075}$,Cr PLNDs (Fig. S4) shows the clear lattice figures, revealing that the ZGO:$Al_{0.075}$,Cr PLNDs are highly crystallized. Size distribution curve in Fig. 2b shows that the ZGO:Al,Cr PLNDs have an average size of about 5 nm. XRD measurements (Fig. S5a) show that ZGO:Al,Cr PLNDs with different concentrations of Al^{3+} all exhibit the same crystal structure as ZGO:Cr. EDS analysis (Fig. S5b) demonstrates the successful doping of Al in the ZGO:Al,Cr PLNDs. These results demonstrate that doping *via* thermal decomposition method did not influence the morphology or crystal structure of the ZGO:Cr PLNDs. The luminescence properties of the ZGO:Al,Cr PLNDs were further investigated. As the concentration of doping Al^{3+} ions increases from 0 to 0.1 at%, the peak intensity at around 700 nm in the phosphorescence spectra of the ZGO:Al,Cr PLNDs increases gradually (Fig. 2c). The gradually enhanced persistent luminescence intensity in the ZGO:Al,Cr PLNDs upon increasing the amounts of doped Al^{3+} ions is further confirmed by the decay images and the fitted decay curves (Fig. 2d and Fig. S6). These results indicate that ZGO:Al,Cr PLNDs with fine-tuned luminescence properties can be prepared through the thermal decomposition method.

Similar results were observed for the Sc^{3+}-doped ZGO:Cr (ZGO:Sc,Cr) PLNDs. TEM images (Fig. 2e and Fig. S7) and size distribution curve (Fig. 2f) show that ZGO:$Sc_{0.075}$,Cr PLNDs have good dispersibility with an average size of about 5 nm. HRTEM image (Fig. S8) show that the ZGO:$Sc_{0.075}$,Cr PLNDs are highly crystallized. The XRD patterns (Fig. S9a) of the ZGO:Sc,Cr PLNDs show that the doping of Sc^{3+} did not influence the crystal structure of the ZGO:Cr PLNDs. EDS analysis (Fig. S9b) further conforms the successful doping of Sc into the ZGO:Sc,Cr PLNDs. The phosphorescence spectra in Fig. 2g suggest that the persistent luminescence intensity of the ZGO:Sc,Cr PLNDs increases with increasing concentration of doping Sc^{3+} ions. Also, it can be further clearly observed in Fig. 2h and Fig. S10 that the persistent luminescence intensity of the ZGO:Sc,Cr PLNDs becomes stronger as increasing the amount of doping Sc^{3+} ions, indicating that the concentration of Sc^{3+} ions could be utilized to modulate the persistent luminescence properties in the ZGO:Cr PLNDs. All these findings demonstrate that thermal decomposition can be utilized as an efficient method for the synthesis of doped persistent nanophosphors, which holds great promise in optimizing the luminescence properties and broadening the applications of persistent nanophosphors.

To test the versatility of the thermal decomposition method in the controlled synthesis of PLNDs, it was further employed to prepare phosphors including sulfide [32,33] and fluoride [34,35] that were previously reported to have persistent luminescence properties. Specifically, two common persistent luminescence phosphors, ZnS:Cr and CaF_2, were prepared with the thermal decomposition method. TEM images in Fig. 3a and Fig. S11 show that the ZnS:Cr PLNDs have excellent dispersibility and exhibit a narrow size distribution with an average size of about 3.5 nm. EDS analysis (Fig. S12a) shows the presence of Cr in the ZnS:Cr PLNDs, suggesting that ZnS:Cr PLNDs were successfully synthesized. The XRD patterns further indicate that the as-synthesized ZnS:Cr PLNDs exhibit the characteristic peaks of standard ZnS crystal (JCPDS 36-1450, Fig. S12b). Fig. 3b shows the phosphorescence spectrum of the ZnS:Cr PLNDs, with a typical emission band of Cr^{3+} ions peaking at around 700 nm. The persistent luminescence decay in the ZnS:Cr PLNDs was measured after pre-excitation by a portable ultraviolet light-emitting diode (LED). Fig. 3c shows that the persistent luminescence in the ZnS:Cr PLNDs can last for more than 30 min. The ultra-long decay feature of the persistent luminescence is also observed in the ZnS:Cr PLNDs through the fitted curve (Fig. S13). The properties of the CaF_2 PLNDs prepared by the thermal decomposition method were also systematically investigated. As shown in Fig. 3d and Fig. S14, the CaF_2 PLNDs display

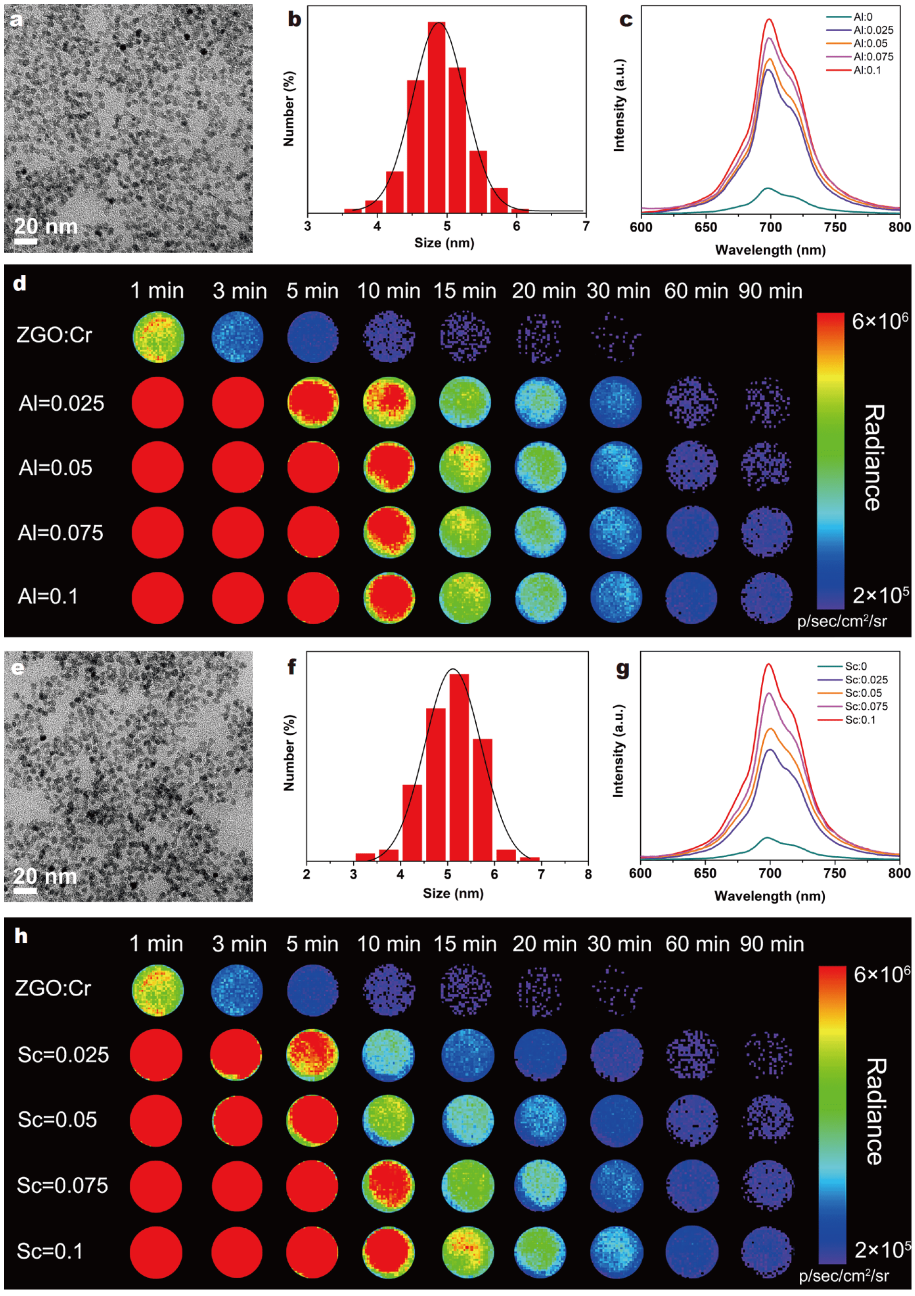

Figure 2 (a) TEM image, (b) size distribution, (c) phosphorescence spectra, and (d) persistent luminescence decay images of the ZGO:Al,Cr PLNDs. (e) TEM image, (f) size distribution, (g) phosphorescence spectra, and (h) persistent luminescence decay images of the ZGO:Sc,Cr PLNDs.

uniform morphology and an ultra-small size of about 2.5 nm. EDS analysis (Fig. S15a) and XRD measurement (Fig. S15b) further demonstrate the CaF_2 PLNDs were successfully synthesized *via* thermal decomposition method. The phosphorescence spectrum in Fig. 3e suggests that the CaF_2 PLNDs show a strong emission band at around 450 nm. In spite of their ultra-small size, the persistent luminescence in the CaF_2 PLNDs can last for more than 1 h (Fig. 3f and Fig. S16), showing their strong ability in trapping the excitation energy for generating persistent luminescence. All these results indicate that thermal decomposition can be used as a versatile method for the synthesis of persistent nanophosphors with good dispersibility, uniform size and strong persistent luminescence. Given that different kinds of persistent nanophosphors possess distinct properties and can meet the

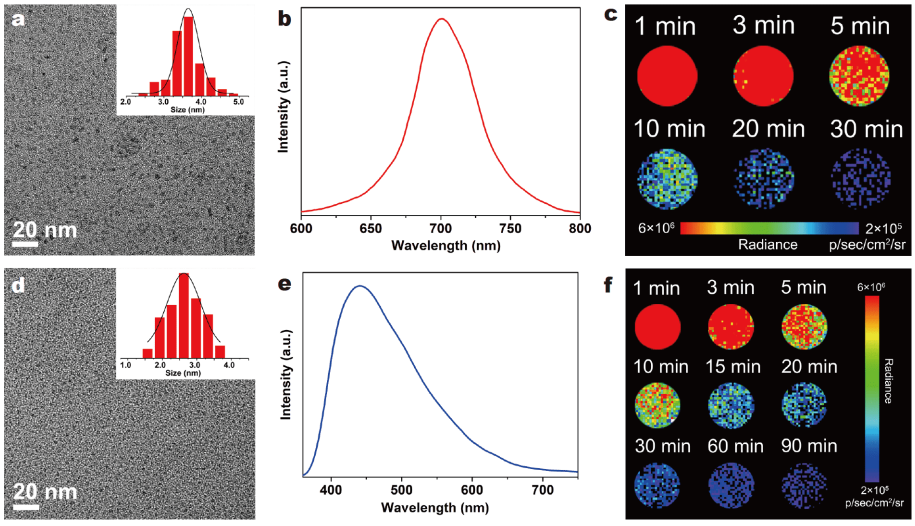

Figure 3 (a) TEM image and size distribution, (b) phosphorescence spectrum and (c) persistent luminescence delay images of the ZnS:Cr PLNDs. (d) TEM image and size distribution, (e) phosphorescence spectrum and (f) persistent luminescence delay images of the CaF_2 PLNDs.

many different requirements in applications, the thermal decomposition method holds great promise in the synthesis of PLNDs for applications ranging from illumination, security sign to bioimaging and cancer therapy.

The biomedical applications of the prepared PLNDs in autofluorescence-free bioimaging were further investigated. Considering their ultra-small size and the surface hydrophobic ligands on the PLNDs, an easy-performed sandwich method was employed to transform the PLNDs from oil phase to aqueous phase [36–39]. Specifically, the ZGO:Al,Cr PLNDs were loaded into the hydrophobic interlayer of liposomes to prepare liposome@ZGO:Al,Cr with good aqueous dispersibility, as illustrated in Fig. 4a. Such integration is expected to combine the excellent biocompatibility of liposomes and persistent luminescence properties of PLNDs. The persistent luminescence decay time of the liposome@ZGO:Al,Cr can reach several minutes and even hours, much longer than the nanoseconds fluorescence lifetime of the biomolecules in biological tissues. Benefiting from such a huge difference in the lifetime, the liposome@ZGO:Al,Cr can effectively eliminate the tissue autofluorescence interference in bioimaging and biosensing. Confocal microscopy and AFM were performed to investigate the constructed liposome@ZGO:Al,Cr nanostructures. As shown in Fig. 4b, the bright field image (left panel) shows that uniform and well-dispersed liposomes are generated. The dark field image (middle panel) presents the circle-shaped luminescence signal of the ZGO:Al,Cr PLNDs. The merged image (right panel) further shows that the luminescence signal exactly locates on the edge of the liposomes, clearly demonstrating that the ZGO:Al,Cr PLNDs are successfully loaded into the hydrophobic interlayer of the liposomes. TEM measurement further shows the ring-like structure of the ZGO:Al,Cr PLNDs within the liposomes, confirming the formation of the liposome@ZGO:Al,Cr nanostructure (Fig. S17). The AFM image in Fig. 4c further presents the uniform and highly dispersed nature of the liposome@ZGO:Al,Cr. The height profiles in Fig. 4d show that the diameter and height of the liposome@ZGO:Al,Cr are about 1 μm and 200 nm, respectively. The persistent luminescence properties of the liposome@ZGO:Al,Cr were further measured. The liposome@ZGO:Al,Cr exhibits obvious persistent luminescence (Fig. S18) and the decay time exceeds 1 h (Fig. 4e and Fig. S19), suggesting their excellent persistent luminescence property. To show the potential applications of the liposome@ZGO:Al,Cr in bioimaging, the liposome@ZGO:Al,Cr was injected into pork tissue at the depth of 1 cm [18,40]. The luminescence decay images of the pork tissue were recorded, as shown in Fig. 4f and Fig. S20. The persistent luminescence signal from the injected liposome@ZGO:Al,Cr is clearly observed without any autofluorescence interference, showing that the liposome@ZGO:Al,Cr can be used in autofluorescence-free bioimaging. Moreover, the persistent luminescence signal can last for more than 10 min, suggesting the good promise of the liposome@ZGO:Al,Cr in long-term bioimaging and bio-tracing. Moreover, it is worth mentioning that the persistent luminescence signal can be detected even at the depth of 1 cm (Fig. 4g), which can be ascribed to the deep tissue penetration ability of the near infrared

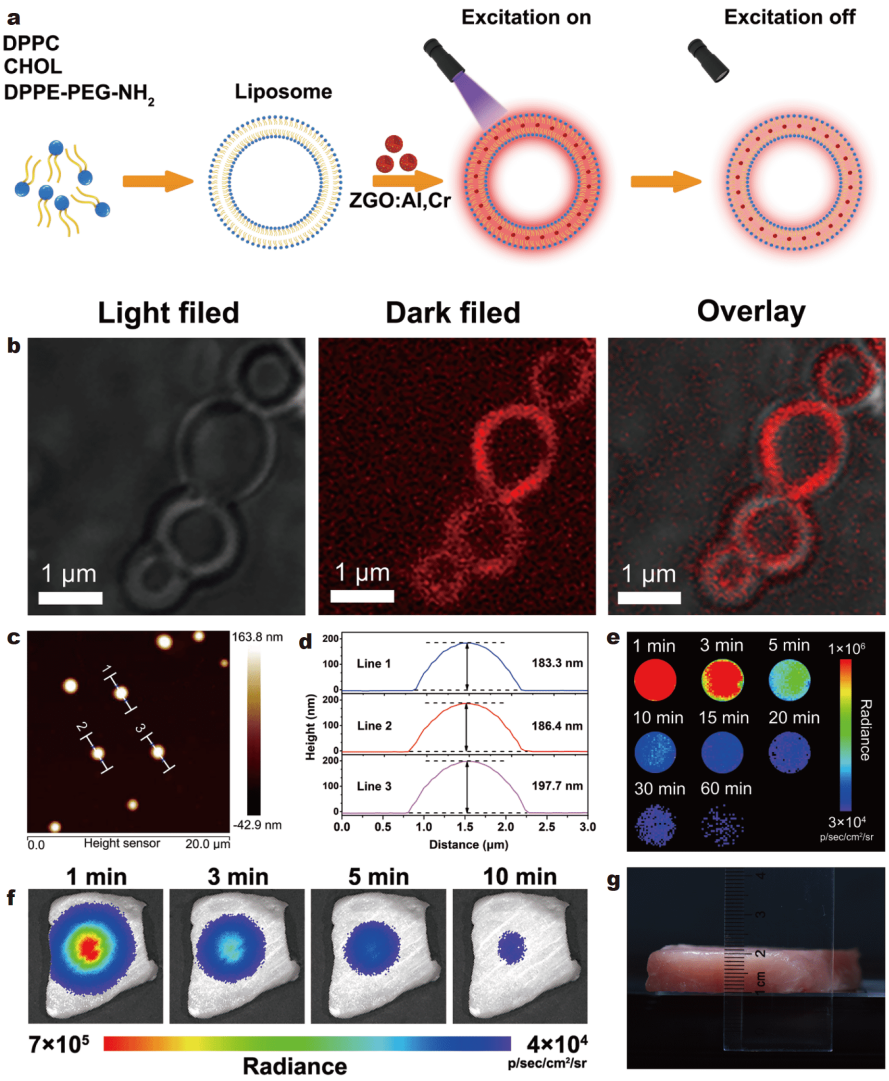

Figure 4 (a) Schematic illustration for the construction of the liposome@ZGO:Al,Cr. (b) Confocal microscopy images of the liposome@ZGO:Al,Cr. (c) AFM image, (d) height profile analysis and (e) persistent luminescence decay images of the liposome@ZGO:Al,Cr. (f) Persistent luminescence decay images of the pork tissue injected with the liposome@ZGO:Al,Cr. (g) Photograph of the pork tissue injected with the liposome@ZGO:Al,Cr.

emission in the liposome@ZGO:Al,Cr. These results suggest that the liposome@ZGO:Al,Cr can be utilized as an excellent autofluorescence-free, deep-tissue and long-term bioimaging platform, holding great promise in disease diagnosis and monitoring of life activities.

CONCLUSIONS

In summary, a general and facile method based on thermal decomposition was developed for the controlled synthesis of ultra-small PLNDs with good dispersibility and bright persistent luminescence. The thermal decomposition method is applicable to the synthesis of gallate, sulfide and fluoride PLNDs. A step further, an easy-performed sandwich method was employed to construct a persistent luminescent nanoplatform based on the ultra-small PLNDs and liposomes. The nanoplatform elegantly integrates the persistent luminescence properties of PLNDs with the good biocompatibility and high loading capacity of liposomes. The developed thermal decomposition strategy opens up a new way for the controlled synthesis of persistent nanophosphors, and it can further promote the applications of persistent nanophosphors. The developed persistent luminescent nanoplatform display good promise in autofluorescence-free deep-tissue bioimaging, and it can be further applied to fields including controlled drug release and imaging-

guided therapy.

Received 7 January 2020; accepted 8 April 2020; published online 27 May 2020

1 Wang J, Ma Q, Zheng W, *et al.* One-dimensional luminous nanorods featuring tunable persistent luminescence for autofluorescence-free biosensing. ACS Nano, 2017, 11: 8185–8191
2 Maldiney T, Bessière A, Seguin J, *et al.* The *in vivo* activation of persistent nanophosphors for optical imaging of vascularization, tumours and grafted cells. Nat Mater, 2014, 13: 418–426
3 Zhao H, Liu C, Gu Z, *et al.* Persistent luminescent nanoparticles containing hydrogels for targeted, sustained, and autofluorescence-free tumor metastasis imaging. Nano Lett, 2020, 20: 252–260
4 Ou X, Chen Y, Xie L, *et al.* X-ray nanocrystal scintillator-based aptasensor for autofluorescence-free detection. Anal Chem, 2019, 91: 10149–10155
5 Zhang KY, Yu Q, Wei H, *et al.* Long-lived emissive probes for time-resolved photoluminescence bioimaging and biosensing. Chem Rev, 2018, 118: 1770–1839
6 Wang Y, Li Z, Lin Q, *et al.* Highly sensitive detection of bladder cancer-related miRNA in urine using time-gated luminescent biochip. ACS Sens, 2019, 4: 2124–2130
7 Wang J, Ma Q, Hu XX, *et al.* Autofluorescence-free targeted tumor imaging based on luminous nanoparticles with composition-dependent size and persistent luminescence. ACS Nano, 2017, 11: 8010–8017
8 Liang L, Chen N, Jia Y, *et al.* Recent progress in engineering near-infrared persistent luminescence nanoprobes for time-resolved biosensing/bioimaging. Nano Res, 2019, 12: 1279–1292
9 Lin Q, Li Z, Yuan Q. Recent advances in autofluorescence-free biosensing and bioimaging based on persistent luminescence nanoparticles. Chin Chem Lett, 2019, 30: 1547–1556
10 Sun SK, Wu JC, Wang H, *et al.* Turning solid into gel for high-efficient persistent luminescence-sensitized photodynamic therapy. Biomaterials, 2019, 218: 119328
11 Sun SK, Wang HF, Yan XP. Engineering persistent luminescence nanoparticles for biological applications: From biosensing/bioimaging to theranostics. Acc Chem Res, 2018, 51: 1131–1143
12 Wang J, Li J, Yu J, *et al.* Large hollow cavity luminous nanoparticles with near-infrared persistent luminescence and tunable sizes for tumor afterglow imaging and chemo-/photodynamic therapies. ACS Nano, 2018, 12: 4246–4258
13 Song L, Li PP, Yang W, *et al.* Low-dose X-ray activation of W(VI)-doped persistent luminescence nanoparticles for deep-tissue photodynamic therapy. Adv Funct Mater, 2018, 28: 1707496
14 Wang J, Ma Q, Wang Y, *et al.* Recent progress in biomedical applications of persistent luminescence nanoparticles. Nanoscale, 2017, 9: 6204–6218
15 Yu N, Li Y, Li Z, *et al.* The "bottom-up" synthesis and applications of persistent luminescence nanoparticles. Sci China Chem, 2018, 61: 757–758
16 Abdukayum A, Chen JT, Zhao Q, *et al.* Functional near infrared-emitting Cr^{3+}/Pr^{3+} co-doped zinc gallogermanate persistent luminescent nanoparticles with superlong afterglow for *in vivo* targeted bioimaging. J Am Chem Soc, 2013, 135: 14125–14133
17 Li Y, Gecevicius M, Qiu J. Long persistent phosphors: from fundamentals to applications. Chem Soc Rev, 2016, 45: 2090–2136
18 Li Z, Zhang Y, Wu X, *et al.* Direct aqueous-phase synthesis of sub-10 nm "Luminous Pearls" with enhanced *in vivo* renewable near-infrared persistent luminescence. J Am Chem Soc, 2015, 137: 5304–5307
19 Zhou Z, Zheng W, Kong J, *et al.* Rechargeable and LED-activated $ZnGa_2O_4:Cr^{3+}$ near-infrared persistent luminescence nanoprobes for background-free biodetection. Nanoscale, 2017, 9: 6846–6853
20 Si R, Zhang YW, Zhou HP, *et al.* Controlled-synthesis, self-assembly behavior, and surface-dependent optical properties of high-quality rare-earth oxide nanocrystals. Chem Mater, 2007, 19: 18–27
21 Lee SS, Zhu H, Contreras EQ, *et al.* High temperature decomposition of cerium precursors to form ceria nanocrystal libraries for biological applications. Chem Mater, 2012, 24: 424–432
22 Zhang X, Wang Y, Cheng F, *et al.* Ultrathin lanthanide oxides nanomaterials: synthesis, properties and applications. Sci Bull, 2016, 61: 1422–1434
23 Zhang M, Zheng W, Liu Y, *et al.* A new class of blue-LED-excitable NIR-II luminescent nanoprobes based on lanthanide-doped CaS nanoparticles. Angew Chem Int Ed, 2019, 58: 9556–9560
24 Homann C, Krukewitt L, Frenzel F, *et al.* $NaYF_4$:Yb,Er/$NaYF_4$ core/shell nanocrystals with high upconversion luminescence quantum yield. Angew Chem Int Ed, 2018, 57: 8765–8769
25 Liang L, Tang Y, Hu X, *et al.* Photoresponsive biomimetic protocells for near-infrared-light-regulated phototheranostics. CCS Chem, 2019, 1: 490–501
26 Hachani R, Lowdell M, Birchall M, *et al.* Polyol synthesis, functionalisation, and biocompatibility studies of superparamagnetic iron oxide nanoparticles as potential MRI contrast agents. Nanoscale, 2016, 8: 3278–3287
27 Si R, Zhang YW, You LP, *et al.* Rare-earth oxide nanopolyhedra, nanoplates, and nanodisks. Angew Chem Int Ed, 2005, 44: 3256–3260
28 Ma Q, Wang J, Zheng W, *et al.* Controlling disorder in host lattice by hetero-valence ion doping to manipulate luminescence in spinel solid solution phosphors. Sci China Chem, 2018, 61: 1624–1629
29 Liang L, Qin X, Zheng K, *et al.* Energy flux manipulation in upconversion nanosystems. Acc Chem Res, 2019, 52: 228–236
30 Yan B. Lanthanide-functionalized metal-organic framework hybrid systems to create multiple luminescent centers for chemical sensing. Acc Chem Res, 2017, 50: 2789–2798
31 Huang P, Zheng W, Gong Z, *et al.* Rare earth ion- and transition metal ion-doped inorganic luminescent nanocrystals: from fundamentals to biodetection. Mater Today Nano, 2019, 5: 100031
32 Wang J, Zhu Y, Grimes CA, *et al.* Multicolor lanthanide-doped CaS and SrS near-infrared stimulated luminescent nanoparticles with bright emission: application in broad-spectrum lighting, information coding, and bio-imaging. Nanoscale, 2019, 11: 12497–12501
33 Gao Y, Li R, Zheng W, *et al.* Broadband NIR photostimulated luminescence nanoprobes based on $CaS:Eu^{2+},Sm^{3+}$ nanocrystals. Chem Sci, 2019, 10: 5452–5460
34 Zheng W, Zhou S, Chen Z, *et al.* Sub-10 nm lanthanide-doped CaF_2 nanoprobes for time-resolved luminescent biodetection. Angew Chem Int Ed, 2013, 52: 6671–6676
35 Yang YM, Li ZY, Zhang JY, *et al.* X-ray-activated long persistent phosphors featuring strong UVC afterglow emissions. Light Sci Appl, 2018, 7: 88
36 Hou Y, Wang C, Chen M, *et al.* Iridium complex nanoparticle mediated radiopharmaceutical-excited phosphorescence imaging. Chem Commun, 2019, 55: 14442–14445
37 Chen C, Gao K, Lian H, *et al.* Single-particle characterization of

theranostic liposomes with stimulus sensing and controlled drug release properties. Biosens Bioelectron, 2019, 131: 185–192
38 Gopalakrishnan G, Danelon C, Izewska P, *et al.* Multifunctional lipid/quantum dot hybrid nanocontainers for controlled targeting of live cells. Angew Chem Int Ed, 2006, 45: 5478–5483
39 Wlodek M, Kolasinska-Sojka M, Szuwarzynski M, *et al.* Supported lipid bilayers with encapsulated quantum dots (QDs) *via* liposome fusion: effect of QD size on bilayer formation and structure. Nanoscale, 2018, 10: 17965–17974
40 Li Y, Zhou S, Dong G, *et al.* Anti-stokes fluorescent probe with incoherent excitation. Sci Rep, 2015, 4: 4059

Acknowledgements This work was supported by the National Natural Science Foundation of China (21925401 and 21904100).

Author contributions Yuan Q and Wang J proposed the research direction and guided the project. Lv X and Chen N designed and conducted the experiments. Lv X wrote the paper with the support from Yuan Q, Wang J and Chen N. All the authors checked the manuscript.

Conflict of interest The authors declare that they have no conflict of interest.

Supplementary information Supporting data are available in the online version of the paper.

Xiaobo Lv obtained his BSc degree from Northeast Forestry University in 2017. He is currently pursuing his Master degree in Prof. Quan Yuan's group at Wuhan University. His interests focus on the controlled synthesis of persistent luminescence nanomaterials and exploring their potential biomedical applications.

Na Chen obtained her BSc and MSc degrees from Hunan University. Later, she joined Prof. Quan Yuan's group at Wuhan University. Currently, she is a PhD candidate in Wuhan University. Her research interest focuses on the controlled synthesis of luminescent nanomaterials for biomedical applications.

Jie Wang obtained his BSc degree from Wuhan Institute of Technology. He obtained his PhD degree in Prof. Quan Yuan's group at Wuhan University. Now he is a postdoctoral fellow in Wuhan University. His research focuses on designing functional luminescence materials for biosensing and bioimaging.

Quan Yuan obtained her PhD degree from Peking University in 2009. Later, she continued her postdoctoral research at the University of Florida. In 2012, she joined Wuhan University as a full professor. Her research focuses on the controlled synthesis of functional nanomaterials and exploring their biomedical applications.

高温热分解法制备亚5 nm的长余辉纳米点用于无背景生物成像

吕小波[1†], 陈娜[1†], 王杰[1], 袁荃[1,2*]

摘要 长余辉是指激发光关闭后发光仍然持续的现象. 长余辉纳米材料在生物医学领域, 尤其是无背景生物成像和光学治疗方面, 表现出巨大的优势. 虽然长余辉材料具有广阔的生物医学应用前景, 但是长余辉纳米材料的控制合成研究非常少. 目前, 长余辉纳米材料基本都是通过煅烧后研磨等"自上而下"的方法制备的, 得到的纳米颗粒分散性差、尺寸不均一、表面难以修饰. 发展长余辉纳米材料的控制合成方法对推进长余辉材料的生物医学应用具有重要价值. 在本文中, 我们提出一种基于乙酰丙酮金属盐的高温热分解方法用于合成超小尺寸的长余辉纳米点. 合成的长余辉纳米点粒径均一, 尺寸在5 nm左右, 具有良好的分散性和明亮的长余辉发光. 通过离子掺杂可以有效地调控长余辉的发光性能. 该方法适用于镓酸盐、硫化物、氟化物等长余辉纳米点的控制合成, 具有良好的普适性. 基于长余辉纳米点的超小尺寸和表面吸附的疏水性配体, 我们构建了脂质体@长余辉纳米点复合生物成像平台, 该平台结合了长余辉纳米点的长寿命发光特点和脂质体的生物相容性好、负载量高等特点, 在生物成像、药物递送等领域有潜在应用价值. 我们的工作为长余辉纳米材料控制合成提供了新思路, 对长余辉纳米材料的生物医学应用具有潜在的推动作用.

